Proceedings of the 16th International Heat Transfer Conference, IHTC-16
August 10-15, 2018, Beijing, China

IHTC16-21877

MONTE CARLO SIMULATION OF SOLAR RADIATION THROUGH A WATER-FILLED PRISMATIC LOUVER

Yaomin Cai[1], Zhixiong Guo[1*], Nicholas Madamopoulos[2]

[1]Dept. of Mechanical and Aerospace Engineering, Rutgers, The State University of New Jersey, 98 Brett Road, Piscataway, NJ 08854, USA
[2]Dept. of Electrical Engineering, The City College of New York, 160 Convent Avenue, New York, NY 10031, USA

ABSTRACT

A Monte Carlo model is developed to simulate the solar radiation transfer through a water-filled prismatic louver for solar energy harvesting. Solar irradiation includes both collimated and diffuse components. The full solar spectrum is divided into different discrete bands for better treatment of the spectral properties of solar irradiation and glass and water absorption. In particular, we considered 1 full band, 3, 7, 10, 20 and 40 bands, respectively. The influences of band division, photon number, and element number on solar energy absorption in the louver are discussed. The energy absorption efficiency utilizing different ratios of collimated and diffuse components is analyzed. For the trade-off of balance between the computational efficiency and accuracy, the 7-band model is generally adopted in most calculations. The effect of mesh division was found to be less sensitive for analyzing the overall solar energy absorption in the louver.

KEY WORDS: Solar irradiation; Radiation absorption; Energy harvest; Modeling; Spectral property

1. INTRODUCTION

The amount of solar irradiation on earth's surface is gigantic: 3×10^{24} joules per year, most of which remains unutilized while we keep depleting traditional fossil fuels [1]. The yearly installation capacity of solar photovoltaic facilities has seen a continuous significant increase worldwide in recent years [2]. The integrated spectral irradiance of ASTM E-490 corresponds to the solar constant which is $E = 1366.1 W/m^2$ above earth's atmosphere [3]. At present, the best reported solar cell is a multi-junction cell having a record of 44.4% efficiency [4]. According to data from EIA (Energy Information Administration), commercial buildings spend more than half total energy on lighting and heating each year [5]. Abundant solar energy can provide natural lighting as well as heating, thus well-utilizing solar energy will lead to energy savings. At present, the majority of green facilities utilizing solar energy only perform either for heating or photovoltaic power generation, making use of only several certain bands of solar irradiation. Most often seen examples are solar water heaters and solar photovoltaic cells. It is needed to develop new technologies to take full advantage of the whole solar spectrum energy.

*Corresponding Author: guo@jove.rutgers.edu

The concept of the proposed glass louver (see Fig. 1) in a glazing system is based on the ability of a prism to deviate the incident light. The collimated solar irradiation will be redirected by the louver to a ceiling and reflected diffusely to a room for illumination. This will minimize "glare effect" and increase natural lighting; and enhanced daylight has the potential to reduce the energy consumption due to artificial lighting for both residential and commercial buildings. On the other hand, the glass and water will absorb the solar energy. The harvested solar energy will be transported and stored as thermal energy in the water, which could be used to replace water heaters or be stored for other purposes. The present study focuses on investigating the efficiency of the solar energy absorption by the proposed water-filled louver.

Monte Carlo (MC) model is a useful simulation method for investigating radiation heat transfer in complex systems [6, 7]. It was applied to thermal radiation problems in the early 1960s [8, 9]. Advantages of using MC include easy handling of complicated physical processes and conditions based on statistical distributions, and easy coding in the construction of computer program without the use of any governing equations. Simulation of radiative energy redistribution in a system is achieved by tracing a large number of energy bundle (photons) from the point of emission till the point of extinction. There are a number of excellent reviews [10 – 14] in the literature on MC methods for radiation transfer in participating media under various conditions. In the present solar-louver system, the solar irradiation on earth surface is highly spectral, and the glass and water absorption and refractive indices are spectrum-dependent. Hence, an MC modelling with appropriate spectral properties incorporating multiple reflection, refraction, absorption, and scattering is necessary.

Recently, the current authors have tackled the problem of solar collimated radiation transfer through the water-filled louver using the MC simulation [15]. Therefore, the present study will be focused on the treatment of solar diffuse irradiation using the MC model. The results combining both collimated and diffuse components will be presented. The solar absorption efficiency and spectrum division for efficient and accurate computation will be scrutinized.

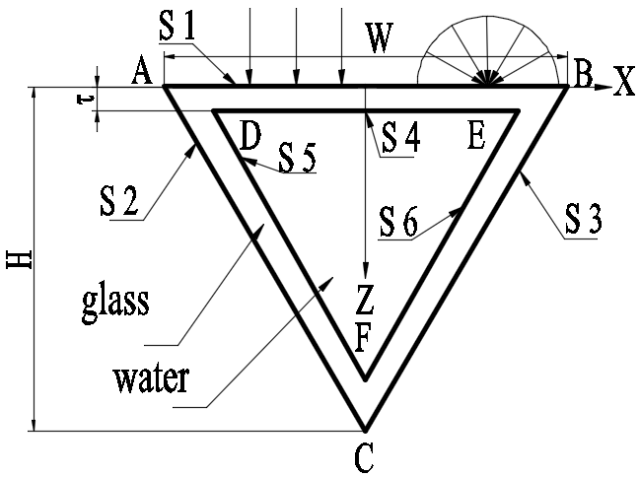

Fig. 1 Sketch of the louver cross-section with solar irradiation from the top

2. SIMULATION METHOD

2.1 Physical model

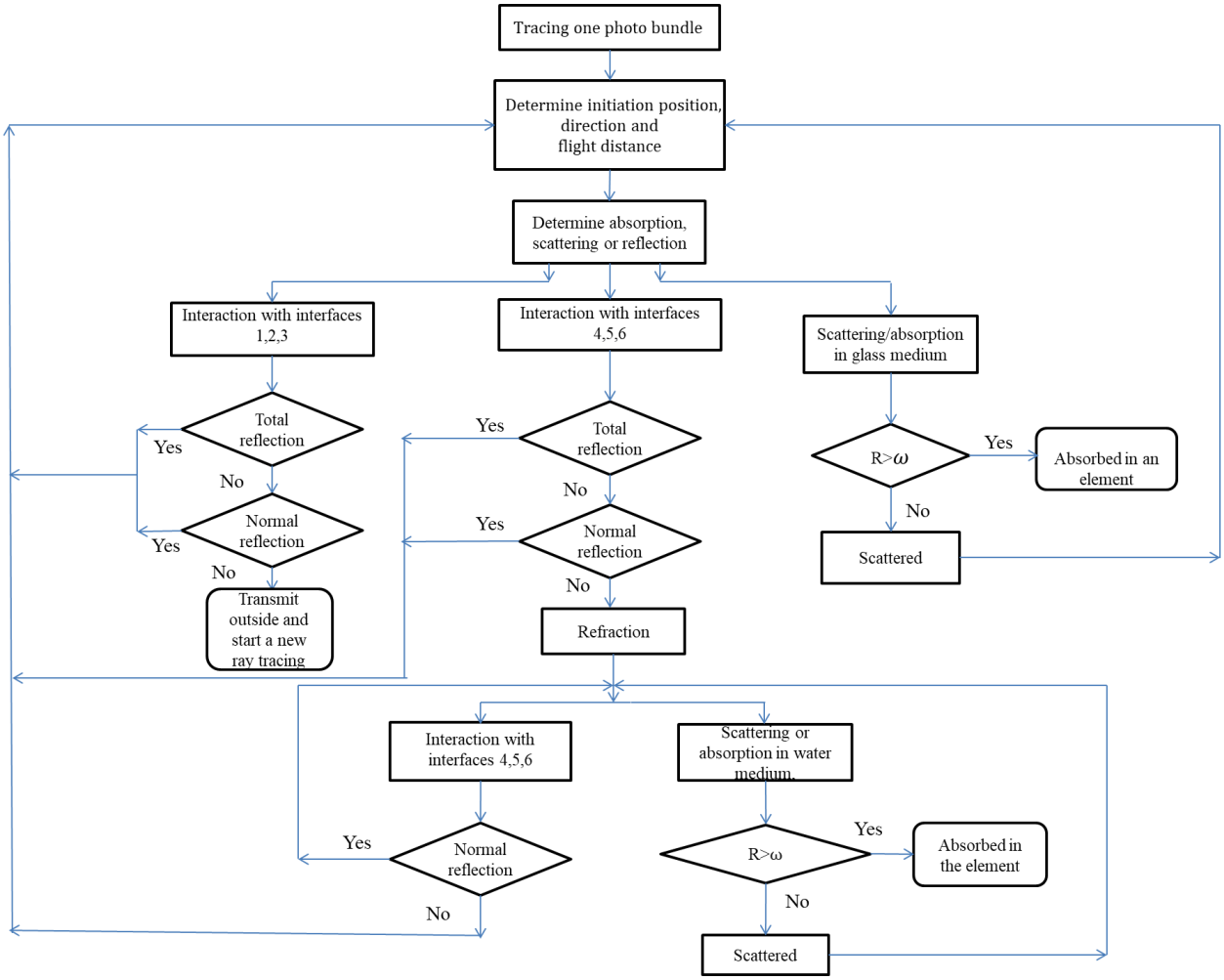

Fig. 2 Flowchart for photon tracing

The physical model discussed in this study is a glazing system consisting of a series of transparent water-filled glass louvers that can be installed on one side of a window to change the direction of collimated sunlight providing natural lighting deeper in the room, as well as to absorb the infrared part in solar radiation to heat the water inside. The cross-section of the prismatic louver is an equilateral triangle, which is assemble of three pieces of uniform silica glass, each with thickness (τ) of 0.125 inches, width (W) of 3 inches, and height (H) of $0.5\sqrt{3}$ W. A brief illustration of the cross-section is plotted in Fig. 1. The only situation that the end effect cannot be neglected is that both θ and $\emptyset$ approach to 90°, which consists of a very small solid angle of incidence. In such a small solid angle, the solar incidence is almost negligible as $\cos\theta$ approaches to zero. Thus, a two-dimensional (2D) geometry is considered in this study. The solar irradiation consisted of both collimated and diffuse components. The collimated radiation is assumed of normal incidence.

2.2 Formulations

Fig. 2 shows the flowchart for tracing one photon bundle in our MC modelling. A photon bundle is initiated

from a position (X_0, Y_0, Z_0) at the solar incident surface of a uniform distribution:

$$X_0 = W * (2i-1)/M - W/2, Y_0 = 0, Z_0 = 0 \quad i=1, 2, \ldots, M \tag{1}$$

where M is the number of total elements on the incident surface.

For diffuse solar irradiation, the incident direction ($\theta_0, \emptyset_0$) is randomly generalized as follows:

$$\theta_0 = \sin^{-1}(\sqrt{R}), \emptyset_0 = 2\pi R \tag{2}$$

where R is the random number. The flight distance, L_β, of a photon bundle is

$$L_\beta = \frac{1}{\beta_\lambda} ln \frac{1}{R} \tag{3}$$

where β_λ is the spectral extinction coefficient of the medium from which the photon is initiated. β_λ is a sum of the spectral absorption coefficient, α_λ, and the spectral scattering coefficient, σ_λ.

There are six interfaces in the louver as shown in Fig. 1, S1- S6. In order to decide which interface the photon bundle will hit or be absorbed/scattered inside the medium, we find the seven possible hitting distances, L_i, and positions by solving

$$\begin{cases} X_i = L_i \sin\theta_0 \cos\emptyset_0 + X_0 \\ Y_i = L_i \sin\theta_0 \sin\emptyset_0 + Y_0 \\ Z_i = L_i \cos\theta_0 + Z_0 \end{cases} \quad i = 1, 2, \ldots, 7 \tag{4}$$

with each of the following functions:

For interaction at surface 1: $Z_1 = 0$ (5a)

For interaction at surface 2: $Z_2 = \sqrt{3}X_2 + H$ (5b)

For interaction at surface 3: $Z_3 = -\sqrt{3}(X_3 - W/2)$ (5c)

For interaction at surface 4: $Z_4 = \tau$ (5d)

For interaction at surface 5: $Z_5 = \sqrt{3}(X_5 + 0.428W) + \tau$ (5e)

For interaction at surface 6: $Z_6 = -\sqrt{3}(X_6 - 0.428W) + \tau$ (5f)

For scattering/absorption in a medium: $L_7 = L_\beta$ (5g)

The distance between the middle point (X_i', Y_i', Z_i') of surfaces S4-S6 and the emission point obeys the rule as follows:

$$L'_i = \sqrt{(X_0 - X_i')^2 + (Y_0 - Y_i')^2 + (Z_0 - Z_i')^2}, \quad i = 4, 5, 6 \tag{6}$$

If $L'_4 \le L'_5$, $L'_4 \le L'_6$ and $L'_5 \le L'_6$, we will check whether the photon will hit S4, S5, S2, S3 and S1 in sequence.

If $L'_4 \le L'_5$, $L'_4 \le L'_6$ and $L'_6 \le L'_5$, we will check whether the photon will hit S4, S6, S3, S2 and S1 in sequence.

If $L'_5 < L'_4$, $L'_5 \le L'_6$ and $L'_4 < L'_6$, we will check whether the photon will hit S5, S4, S3, S1 and S2 in sequence.

If $L'_5 < L'_4$, $L'_5 \le L'_6$ and $L'_6 < L'_4$, we will check whether the photon will hit S5, S6, S3, S1 and S2 in sequence.

If $L'_6 < L'_4$, $L'_6 < L'_5$ and $L'_4 < L'_5$, we will check whether the photon will hit S6, S4, S1, S2 and S3 in sequence.

If $L'_6 < L'_4$, $L'_6 < L'_5$ and $L'_5 < L'_4$, we will check whether the photon will hit S6, S5, S2, S1 and S3 in sequence.

Further, if $L_\beta \ge L_4 > 0$ and $X_D \le X_4 \le X_E$, the photon will hit S4; if $L_\beta \ge L_5 > 0$ and $X_D \le X_5 \le X_F$, it will hit S5; if $L_\beta \ge L_6 > 0$ and $X_F \le X_6 \le X_E$, it will hit S6; if $L_\beta \ge L_2 > 0$ and $0 \le X_2 \le X_C$, it will hit S2; if $L_\beta \ge L_3 > 0$ and $X_C \le X_3 \le X_B$, it will hit S3; if $L_\beta \ge L_1 > 0$ and $0 \le X_1 \le X_B$, it will hit S1;

otherwise, it will be absorbed or scattered in the glass medium.

If the photon starts inside the water medium due to scattering, justify the following: if $L_\beta \geq L_4 > 0$ and $X_D \leq X_4 \leq X_E$, it will hit S4; if $L_\beta \geq L_5 > 0$ and $X_D \leq X_5 \leq X_F$, it will hit S5; if $L_\beta \geq L_6 > 0$ and $X_F \leq X_6 \leq X_E$, it will hit S6; otherwise, the photon will be absorbed or scattered in the water medium.

If a photon hits a surface, we need to consider whether the photon will reflect or transmit. For reflection, specular reflection condition is adopted as the surfaces are smooth. For refraction, Snell's law is employed:

$$n_i \sin\theta_i = n_r \sin\theta_r \tag{7}$$

where n_i and n_r are refractive indices of a medium in the incoming and refractive sides, θ_i and θ_r represent the incident angle and angle of refraction, respectively.

If $n_i > n_r$, there exists a critical angle, θ_c, defined by

$$\theta_c = sin^{-1}\left(\frac{n_r}{n_i}\right) \tag{8}$$

When $\theta_i \geq \theta_c$ and the incident radiation is totally reflected with specular reflection condition.

The reflectivity of incident radiation on an interface is given by Fresnel equation:

$$\rho = \frac{1}{2}\left[\frac{tan^2(\theta_i-\theta_r)}{tan^2(\theta_i+\theta_r)} + \frac{sin^2(\theta_i-\theta_r)}{sin^2(\theta_i+\theta_r)}\right] \tag{9}$$

where ρ is the reflectivity; θ_i and θ_r represent the angle of incidence and angle of refraction, respectively. If $R < \rho$, the photon will reflect; otherwise, it will transmit.

The ray vector $\overrightarrow{V_r}$ after reflection is

$$\overrightarrow{V_r} = \overrightarrow{V_i} + 2(|\overrightarrow{V_i}| \cos\theta_i) \cdot \vec{n} \tag{10}$$

where $\vec{n}$ is the normal direction outward the hitting surface, $\overrightarrow{V_i}$ is the incoming ray vector. The ray vector after refraction, $\overrightarrow{V_t}$, is

$$\overrightarrow{V_t} = \frac{tan\,\theta_r}{tan\,\theta_i}\left[\overrightarrow{V_i} + \vec{n}\left(\overrightarrow{V_i} \cdot \vec{n}\right)\right] - \vec{n}\left(\overrightarrow{V_i} \cdot \vec{n}\right) \tag{11}$$

Once we obtained the ray vector after refraction/reflection, we can get θ and $\emptyset$, respectively.

To trace the reflected/refracted photon, a reduced flight distance is used and calculated as the difference between the originally-calculated flight distance and the flight distance between photon initiating and the hitting surface. If refraction occurs, the transformation between two different media is calculated by

$$L'_{1\beta}\beta_{1\lambda} = L'_{2\beta}\beta_{2\lambda} \tag{12}$$

where $L'_{1\beta}$ is reduced flight distance in the same medium, $L'_{2\beta}$ is the reduced flight distance in another medium after refraction. For scattering, a new flight distance will be calculated based on Eq. (3).

If the photon is absorbed or scattered, we use the scattering albedo to determine whether the photon is absorbed or scattered. If $R < \omega$, in which ω is the scattering albedo, the photon would scatter; otherwise, it would be absorbed. The new scattering direction is determined by isotropic scattering condition in this study, as water scattering is very weak and glass scattering is negligible, given by:

$$\theta_1 = cos^{-1}(1-2R), \quad \emptyset_1 = 2\pi R \tag{13}$$

where θ is the new azimuthal angle and $\emptyset$ is the new circumferential angle.

The spectral divergence of heat flux, $Q_{\lambda i}$, due to solar diffuse irradiation for an element i is calculated by

$$Q_{\lambda i} = \sum_{j=1}^{N_{\lambda i}} (1 - \rho_{j\lambda}) \frac{W \times E_\lambda}{S_i \times NRAY} \quad (14)$$

where $N_{\lambda i}$ is the absorbed spectral photon number in the element; S_i is the cross-sectional area of the element; NRAY is the total photon bundles number refracted from the inward surface of solar incidence; E_λ is the diffuse spectral solar heat flux on the louver's out surface; and $\rho_{j\lambda}$ is the spectral surface reflectivity of light from air to silica glass on j photon penetrating. The total divergence of diffuse irradiation, Q_{1i}, is an integral of the spectral value, i.e., the sum of contributions from all the solar bands:

$$Q_{1i} = \frac{W \times E}{S_i} \sum_{\lambda=280}^{4000} \sum_{j=1}^{N_{\lambda i}} \frac{(1-\rho_{j\lambda})}{NRAY} w_\lambda \quad (15)$$

where E is the diffuse solar heat flux on the louver's out surface and w_λ is the energy weighting factor of a spectral band.

Since the solar heat flux varies depending on location, season, day and time, it would be more convenient to show the energy absorption in terms of normalized energy harvest Q_{1i}' defined as:

$$Q_{1i}' = \frac{Q_{1i}}{E_1} \quad (16)$$

The energy absorption efficiency for diffuse irradiation is defined as:

$$\epsilon_1 = \sum_i \sum_{\lambda=280}^{4000} \sum_{j=1}^{N_{\lambda i}} \frac{(1-\rho_{j\lambda})}{NRAY} w_\lambda \quad (17)$$

We compare absorption efficiency in the glass and water respectively. The total efficiency is a sum of these two contributions.

Similarly, we considered solar energy absorption for collimated solar irradiation in our previous study [15]. The whole solar energy consists of diffuse and collimated components. Suppose the diffuse component ratio is α_1, and Q_{2i} is the contribution due to collimated irradiation, then the local divergence of whole heat flux, Q_{3i}, for a single element would be

$$Q_{3i} = Q_{1i} + Q_{2i} \quad (18)$$

The total normalized energy harvest Q_{3i}' would be

$$Q_{3i}' = \alpha_1 \times Q_{1i}' + (1 - \alpha_1) \times Q_{2i}', \quad (19)$$

And the total efficiency would be:

$$\epsilon_{total} = \alpha_1 \epsilon_1 + (1 - \alpha_1) \epsilon_2 \quad (20)$$

where ϵ_2 is the absorption efficiency for collimated irradiation.

Solar irradiation is highly spectral, and so are the properties of water and glass. The details of different spectral optical properties on different bands can be found in our recent paper[15].

2.3 Elements and bands division

The louver was divided into 462, 1,086, 4,032, 7,140 and 11,130 elements respectively. A brief illustration of a representative mesh with 462 elements is shown in Fig. 3.

Solar irradiation is highly spectral, and so are the properties of water and glass in the whole solar spectrum ranging from 280 – 4,000nm. Both glass and water are highly absorbing medium against solar spectrum. Scattering in the glass is negligible and extremely weak in water. However, spectral variation in refractive index is not negligible for both glass and water. Further, there exists mismatch of refractive indices in the interfaces between glass/air and glass/water. We tried to divide the solar spectrum into discrete bands, and band-averaged properties are used in our calculations. We divided the spectrum in a way such that property

profiles are relatively smooth within each band. Another factor considered was that each band contains a similar amount of solar energy to keep close weight. So the bandwidth varies along the full solar spectrum: in a region with condensed energy, such as the visible and near-infrared regions, the bandwidth is relatively narrower. A single air mass value of 1.5 from ASTM Standard G173-03 [16] was adopted in calculating the solar irradiation on earth's surface. The details about the bands' division were listed in a table in our recent article [15], in which we considered 1 full band, 3, 7, 10, 20, and 40 bands, respectively.

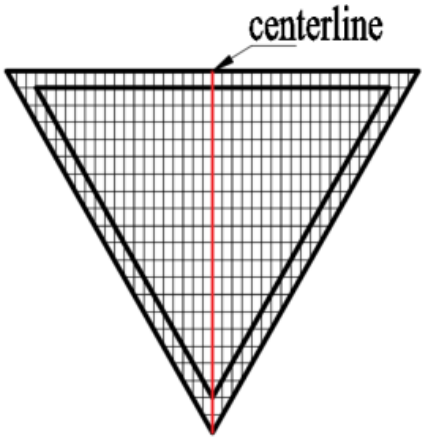

Fig. 3 A representative nodes division

3. Results and Discussion

First, we validate the MC calculations for solar diffuse irradiation under different photon numbers. Four sets of photon numbers were considered, i.e., $10^6, 10^7, 10^8$ and 10^9 photons. Fig. 4 compares the normalized energy harvest for different photon numbers. It is seen that a large amount of solar energy will be absorbed in the incident glass layer. The absorbed energy decreases significantly as the photon going deep in the water region. Fig. 5 plots the contours for the four calculation cases considered in Fig. 4. We used Inter® Core™ i-7-4720HQ CPU@ 2.60GHz for calculations. 2819.0s was spent for 10^8 photons and 28679.2s for 10^9 photons simulations, respectively. Hence, 10^8 photons seem to be suitable for computational accuracy and efficiency.

Next, we examine the effect of element division. We considered meshes of 462, 1,086, 4,032, 7,140 and 11,130 elements for comparison. In the calculations, 10^8 photons and 7 bands were employed. Fig. 6 shows the solar energy absorption efficiencies in glass region, water region, and the whole louver region, respectively. It is seen that element division does not affect these three efficiencies. Absorption by the glass is much stronger than by the water inside the louver. Figs. 7 and 8 examine the local solar absorption. It is seen that the element division affects local distribution of solar energy absorption. It took 2804.6s for 462 elements, 2877.7s for 1,086 elements, 2804.6s for 4,032 elements, 2819.0s for 7,410 elements and 2878.33s for 11,130 elements. Combining the computation efficiency and accuracy, this model with 7,140 elements will be adopted in later calculations.

Band division is a very important issue for accurate and efficient modeling of solar irradiation. We considered the solar spectrum as a full band, 3, 7, 10, 20 and 40 bands, respectively. Fig. 9 shows the total/glass/water solar energy absorption efficiencies for different band divisions. It is seen that the absorption efficiency generally decreases as increasing band numbers, except for the case from 1 band to 7 bands for glass.

However, the variation after 7 bands is very small. Fig. 10 shows the normalized energy harvest distributions along the centreline. Again the results from the 1-band and 3-band divisions deviate largely from other cases. The division of 7 bands is acceptable. Fig. 11 shows the contours of normalized energy harvest in the whole louver. It shows that 1-band and 3-band situations have a larger absorption in the glass, i.e., the solar irradiation is heavily attenuated by the incident glass layer. The 7-band would be a good choice as its result is similar to the 10-, 20-, and 40-band models. Since the CPU time is linearly proportional to band number. The 7-band model is used in the present study.

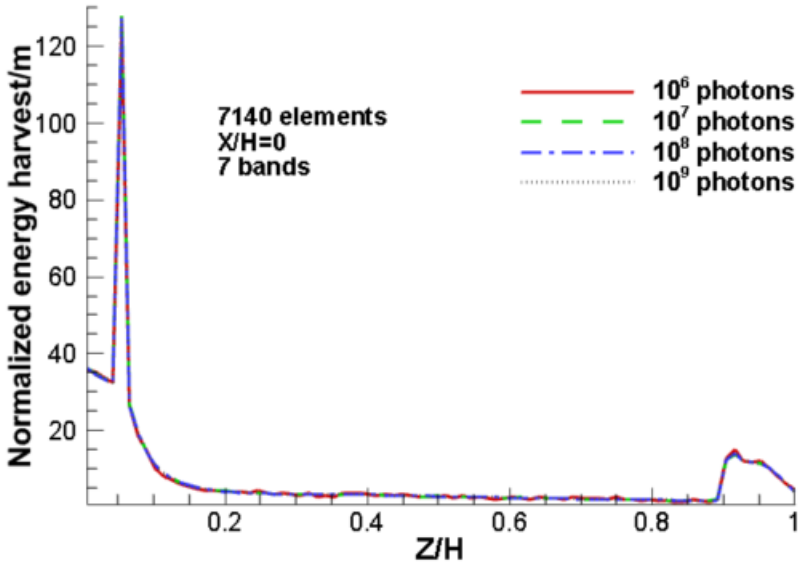

Fig. 4 Normalized energy harvest (/m) along the centerline for different photon numbers

Now we utilized 7-band and 10^8 photons model to analyse the influence of combined diffuse and collimated solar irradiation. It is well known that the ratio of a diffuse component over the total irradiation (diffuse + collimated) varies with location, season, day, time, and weather conditions. In the present study, we just considered one situation for the collimated irradiation, i.e., the incidence is normal to the louver surface. The paper adopted $0.2, 0.4, 0.6$ and 0.8 as the ratios of the diffuse irradiation to total irradiation to see the total/glass/water energy absorption efficiencies and the normalized energy distribution contours for the louver.

Fig. 12 shows that absorption efficiency against the variation of diffuse component. It is seen that as the diffuse irradiation ratio increases, the total/glass/water energy absorption efficiencies decrease. Fig. 13 plots the contours of normalized energy harvest for four different ratios of diffuse irradiation. It is seen that the value in the region of the bottom tip reduces as the diffuse component increases. It implies that the diffuse irradiation cannot penetrate as deeper as the collimated irradiation.

4. CONCLUSIONS

The absorption of solar irradiation with both the collimated and diffuse components within a water-filled prismatic louver is investigated using the MC method. In particular, the spectral features of solar irradiation and

material properties are considered. The method is validated via intensive comparisons among the use of different photon numbers, element numbers, and band division numbers. Some conclusions can be drafted as follows:

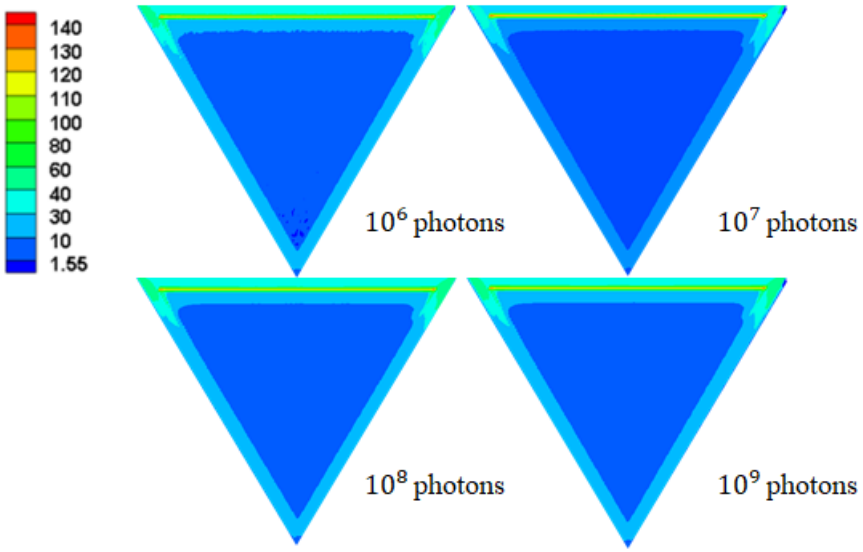

Fig. 5 Contours of normalized energy harvest (/m) for different photon numbers

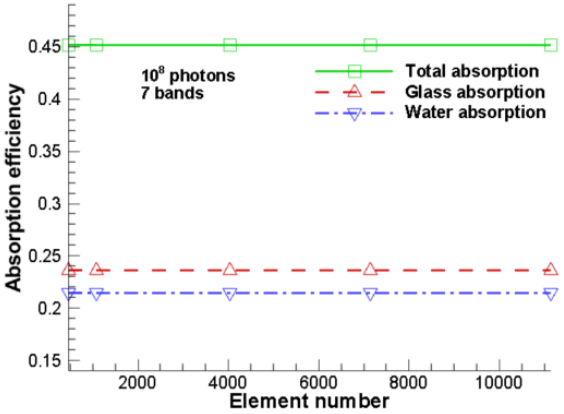

Fig. 6 Solar energy absorption efficiency vs. elements division

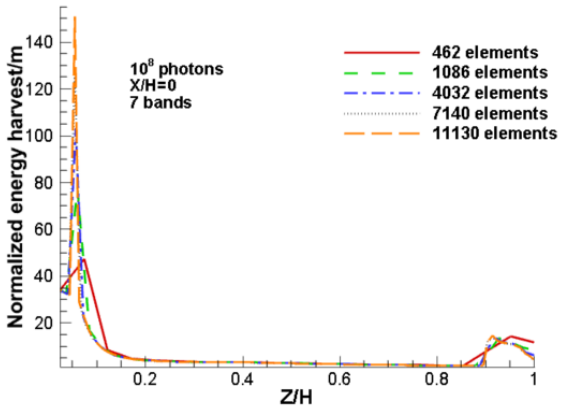

Fig. 7 Normalized energy harvest (/m) along the centerline for different element numbers

1. The overall solar energy harvested in the water and glass regions is a weak function of element division. However, the precise local distribution of energy deposition does depend on the element division. A finer mesh will get a better symmetric profile in the louver. As the water inside the louver is moving, the division of meshes will be critical in the combined modeling of heat and fluid flow in the future.

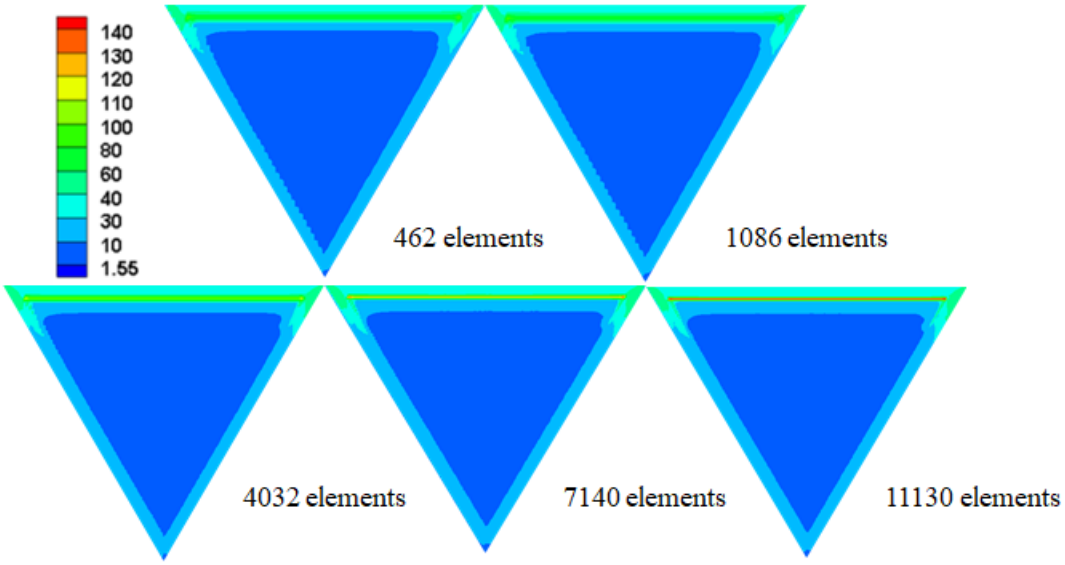

Fig. 8 Contours of normalized energy harvest (/m) for different element divisions

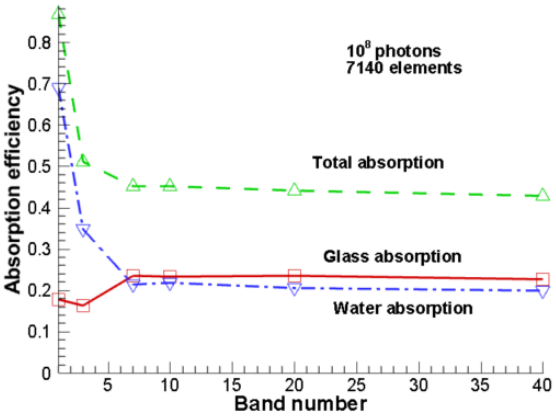

Fig. 9 Solar energy absorption efficiency vs. band divisions

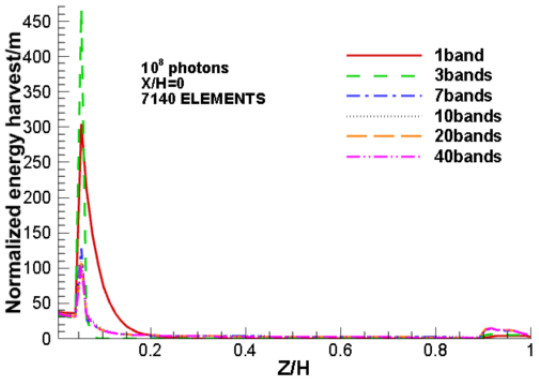

Fig. 10 Normalized energy harvest along the centerline for different band numbers

2. Adopting the solar spectrum as a full band or 3-band is not good enough for accurately simulating the solar radiation transfer through glass and water. The 7-band model works well as compared with the 10-, 20-, and 40-band models. It is also computational efficient as compared with the large band number cases.
3. The louver energy absorption to the diffuse solar irradiation is weaker than to the normally incident collimated irradiation. Thus, the louver would be better to face directly the solar irradiation.

Future work should investigate the influence of different latitudes, seasons, and climatic conditions on both the collimated and diffuse solar radiation.

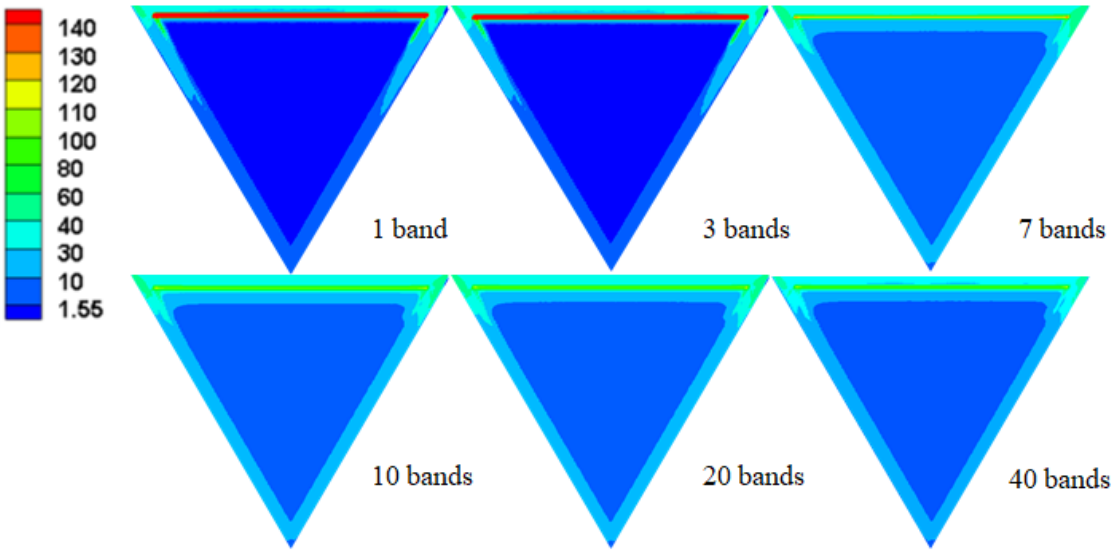

Fig. 11 Contours of normalized energy harvest (/m) with different bands

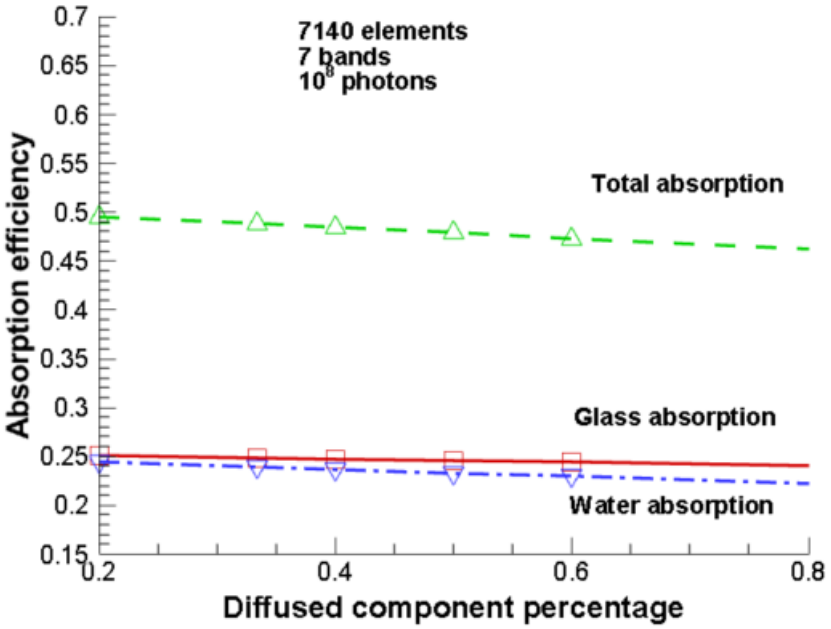

Fig. 12 Solar energy absorption efficiency for different ratios of diffuse component

ACKNOWLEDGMENTS

This material is based upon work supported by the National Science Foundation under grant No. ECCS-1505706. Y.C. acknowledges fellowship from the China Scholarship Council (CSC) for study at Rutgers University.

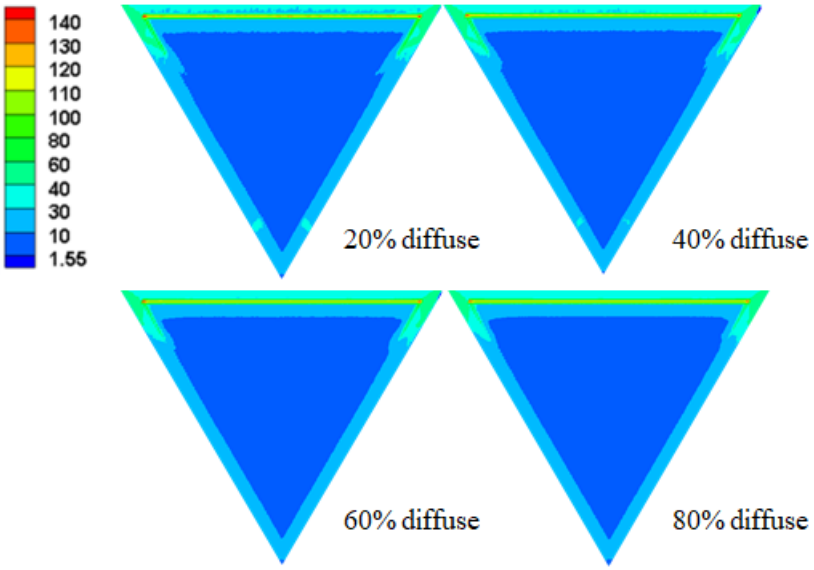

Fig. 13 Contours of normalized energy harvest (/m) for different ratios of diffuse irradiation

NOMENCLATURE

E	diffuse solar heat flux	(w/m^2)
E_λ	diffuse spectral solar heat flux	(w/m^2)
N_i	absorbed photons in a single element	
NRAY	total emission photons	
$N_{\lambda i}$	absorbed spectral photon number in the element	
W	width of the louver	(m)
w_λ	spectral weighting factor	
L_β	total photon flight distance in the glass medium	(m)
L'_β	new flight distance after scattering /reflection/refraction	(m)
$L'_{1\beta}$	reduced flight distance in the same medium	(m)
$L'_{2\beta}$	reduced flight distance in the another medium	(m)
$Q_{\lambda i}$	spectral divergence of heat flux for element i	(m^{-1})
Q_{1i}	diffuse component divergence of	
$\overrightarrow{V_i}$	the incoming ray vector	
$\overrightarrow{V_r}$	ray vector after reflection	
$\overrightarrow{V_t}$	ray vector after refraction	
α_1	diffuse component ratio	
α_λ	absorption coefficient	(m^{-1})
ϵ_1	absorption efficiency for diffuse irradiation	
ϵ_2	absorption efficiency for collimated irradiation	
ϵ_{total}	total absorption efficiency	
ω	scattering albedo	
$\emptyset$	circumferential angle after reflection or refraction	(degrees)
$\emptyset_0$	circumferential angle for MC	(degrees)
$\emptyset_1$	scattering circumferential angle	(degrees)
ρ	reflectivity	
$\rho_{j\lambda}$	spectral surface reflectivity of j photon penetrating	
σ_s	scattering coefficient	(m^{-1})

	energy harvest (w/m^3)	θ	azimuthal angle after reflection or refraction (degrees)
Q'_{1i}	diffuse component normalized energy harvest (m^{-1})	θ_0	azimuthal angle for MC simulation (degrees)
Q_{2i}	collimated component divergence of heat flux (w/m^3)	θ_1	scattering azimuthal angle (degrees)
Q'_{2i}	collimated component normalized energy harvest (m^{-1})	θ_i	incident angle (degrees)
Q_{3i}	local divergence of whole heat flux (w/m^3)	θ_r	refractive angle (degrees)
Q'_{3i}	whole normalized energy harvest (m^{-1})	θ_c	critical angle (degrees)
		S_i	cross-sectional area of the element (m^2)
		S	area that the sunlight can direct irradiate with (m^2)

REFERENCES

[1] Smil, V., *Oil: A Beginner's Guide*, London: Oneworld Publications, (2008).

[2] Wiesenfarth, M., Helmers, H., Philipps, S. P., Steiner, M., and Bett, A. W., "Advanced Concepts in Concentrating Photovoltaics (CPV)," *Proc. 27th European PV Solar Energy Conf. and Exhi.*, pp. 11-15, (2012).

[3] ASTM-E490-00a, *Standard Solar Constant and Zero Air Mass Solar Spectral Irradiance Tables*, ASTM International, West Conshohocken, PA, (2000)).

[4] Green, M. A., Emery, K., Hishikawa, Y., Warta, W., and Dunlop, E. D., "Solar Cell Efficiency Tables (Version 45)," *Prog. Photovolt: Res. Appl.*, 23, pp. 1–9, (2015).

[5] Duffie, J. A. and Beckman, W. A., *Solar Engineering of Thermal Processes*, 4th ed., Hoboken: John Wiley & Sons, (2013).

[6] Siegel, R. and Howell, J. R., *Thermal Radiation Heat Trans., 4th ed*. Taylor & Francis, New York, (2001)

[7] Modest, M. F., *Radiative Heat Transfer*, 3rd ed., New York: Academic press, (2013).

[8] Howell. J. R. and Perlmutter, M., "Monte Carlo Solution of Thermal Transfer Through Radiant Media Between Gray Walls," *J. Heat Transf.*, 86(1), 116-122, (1964).

[9] Taniguchi, H., "Temperature Distributions of Radiant Gas Calculated by Monte Carlo Method," *Bulletin of JSME*, 10, pp. 975-988, (1967)

[10] Yang, W. J., Taniguchi, H., Kudo, K., "Radiative Heat Transfer by the Monte Carlo method," *Adv. Heat Transf.*, 27, pp. 1-215, (1995).

[11] Farmer, J. T. and Howell, J. R., "Comparison of Monte Carlo Strategies for Radiative Transfer in Participating Media," *Adv. Heat Transf.*, 31, pp. 333-429, (1998).

[12] Walters, D. V., and Buckius, R. O., "Monte Carlo Methods for Radiative Heat Transfer in Scattering Media," *Annual Rev. Heat Transf.*, 5.5, (1994).

[13] Kaminski, D. A. , "Radiative Transfer from a Gray, Absorbing-emitting, Isothermal Medium in a Conical Enclosure," *J. Sol. Energy Eng.*, 111, pp. 324-329 , (1989).

[14] Guo, Z., Kumar, S., and San, K. C., "Multidimensional Monte Carlo Simulation of Short-pulse Laser Transport in Scattering Media," *J. Thermophysics Heat Transf.*, 14, pp. 504-511, (2000).

[15] Cai, Y. M. and Guo, Z., "Spectral Monte Carlo simulation of collimated solar irradiation transfer in a water-filled prismatic louver," *Appl. Opt.*, 57, pp. 3021-3030, (2018)

[16] ASTM G173-03, *Standard Tables for Reference Solar Spectral Irradiances: Direct Normal and Hemispherical on 37 Tilted Surface*, ASTM International, West Conshohocken, PA, (2003).